# On the exploitation of polarimetric ratio for oil spill detection

Mariantonietta Zonno(*), Mariantonietta.Zonno@dlr.de, +49-8153-28-3112
Paco López-Dekker(*), Francisco.LopezDekker@dlr.de
Richard E. Danielson(**), Rick.Danielson@nersc.no

(*) German Aerospace Center (DLR), Microwaves and Radar Institute, Muenchner Strasse 20, 82234 Wessling, Germany
(**) Nansen Environmental and Remote Sensing Center (NERSC), Norway

## Abstract

Oil spills in sea water represent one of the most conspicuous forms of damage to the marine environment. They can be detected in SAR images by the exploitation of the normalized cross section (NRCS) and the co-polarization ratio (PR) and by the use of a combined detector. In this paper we describe the simulation of sea surface SAR data by means of the statistical compound model and we use these data for testing the proposed NRCS and PR-based oil spill detection approach. It shows good performance compared to detectors based on the single PR or NRCS information.

## 1 Introduction

The largest oil spills accidents, caused by several hundred thousand tons of crude oil and refined fuel spilled from tanker ships or platforms, have damaged natural ecosystems in Kuwait, Alaska, Gulf of Mexico, Galapagos Islands and France. Nevertheless, smaller spills such as oil releases from ships in transit as well as produced water containing small amounts of oil from off-shore oil installations, account for over 20% of the total oil pollution and have proven to have a great impact on the ecosystems because of the remoteness of the site or the difficulty of an emergency environmental response.

SAR systems have been employed for ocean pollution monitoring thanks to their day and night, weather independent acquisitions, together with the capability of imaging wide areas, up to hundreds of kilometers, with high-resolution [1, 2].

Oil spills cause the damping of the small scale surface structures and appear in SAR intensity images as areas of reduced backscatter compared to the surrounding sea. This characteristic has been commonly exploited in conventional oil spill detection services: the low backscattering level of oil spills suggests the use of thresholding methods, as in [3, 4]. However, natural phenomena such as low wind areas, rain cells, shear zones, ship wakes, natural films, may appear as dark spots in SAR images leading to misinterpretations and limiting the accuracy of the monitoring services. They are called look-alikes. Some additional oil features, such as geometry and shape and texture (see for example [3, 5]) may be extracted from the darker spots in the SAR single-pol images, and provided as further inputs to an oil detector in order to improve the classification capabilities.

There is also growing evidence that fully polarized Normalized Radar Cross Section (NRSC) allows a better distinction between Bragg scattering, wave breaking, and oil spills [6]: thus, an increasing interest towards the exploitation of polarimetric features for oil spills detection has been shown by the scientific community ([7, 8]). This paper deals with a comparison of two Constant False Alarm Rate (CFAR) detectors for oil spill, based on NRCS and co-polarization ratio. It is defined as the ratio of the radar cross section for the two polarimetric channels $(\sigma_{VV}/\sigma_{HH})$ and is here proposed to have a distinctive characteristic for oil spill. Additionally, a combined CFAR detector, exploiting both the NRCS and the PR information for oil and sea water has been tried out, revealing better performance than the single detectors and showing probabilities of detection reaching one for different sea states. The analysis has been based on simulated data generated according to the statistical models for the sea and properly modified for the oil.

## 2 Sea and oil spill model

### 2.1 Physical model for sea surface backscattering

Radar backscatter from the sea is the result of a complex interaction between incident electromagnetic waves and sea surface. It is still nowadays very difficult to find a general model in agreement with all the possible observations depending on the combination of sea state (winds and waves) and radar system frequency, polarization and incidence angle. In the model proposed by [9], the total radar scattering from the sea is the result of contributions from regular wavy surface and breaking zones, which are statistically independent. The radar backscattering from the regular surface is actually the sum of two different scattering mechanisms: specular reflection and (resonant) Bragg scattering, according to the composite model. The total NRCS of the sea surface $\sigma_0$ is then:

$$\sigma_0 = (\sigma_{0Spec} + \sigma_{0Bragg}) \cdot (1 - q) + \sigma_{Break} \cdot q \quad (1)$$

ISBN 978-3-8007-4228-8 / ISSN 2197-4403

where $q$ is the portion of sea surface affected by breaking waves while $(1-q)$ the regualar one, and $\sigma_{0Spec}$, $\sigma_{0Bragg}$ and $\sigma_{0Break}$ are, respectively, the NRCS due to specular, Bragg and breaking waves scattering.
At smaller incident angles, specular reflection is the main scattering mechanism; it changes according to the surface roughness and is generated by surface waves with wavelengths 3 to 10 times larger than the radar wavelength. On the contrary, the scatterers contributing to $\sigma_{0Bragg}$ are short surface waves that are spatially resonant with the incident electromagnetic waves. According with the two scale model (see [10]), the Bragg waves are superimposed on longer tilting waves. Finally, the breaking waves scattering can be thought as specular reflections from very rough wave patterns.

## 2.2 Oil slicks radar measurements

The presence of oil over the sea surface modify the seawater viscosity and damps the small scale structures (capillary waves) and Bragg scattering. The visible effect in the SAR images is a lower backscatter from oil covered areas resulting in darker patches in comparison with the surroundings. Apparently, the contrast between oil and no-oil areas makes easy the oil spill detection in SAR images. In the reality, the accuracy is strongly affected by the presence of look-alikes, such as natural films, low wind areas, rain cells, shear zones and ship wakes. Furthermore, the oil slicks detection capability is function of several radar, ocean and oil parameters. Different experiments have shown that [11]:

- slicks show higher contrast at C, X, and Ku bands rather than at lower frequencies (S and L band).
- The most suitable incidence angle range is between 20 and 45 degrees; in this range it is easier to identify the damping effect of the shorter waves caused by the presence of the oil.
- The choice of polarization depends on the other factors, such as radar frequency and wind speed. For C band and stronger wind, VV suits better for the oil spill detection.
- The higher the oil elasticity and thickness, the more evident the contrast in SAR images.

### 2.2.1 Co-polarization ratio

Nonetheless the exploitation of the dual/quad polarimetric capabilities of some SAR systems allows a more extended characterization of the oil slicks. Specifically, the co-polarization ratio (hereinafter PR), defined as the ratio of the radar cross section for the two polarimetric channels $(\sigma_{VV}/\sigma_{HH})$, shows smaller values for oil slicks than for sea. In [12] this is physically justified by a lower dielectrical constant of the oil compared to the seawater while, in [6] it is is demonstrated the PR helps to distinguish Bragg scattering from breaking waves. Thus, there is a potential for the PR to be exploited also for oil spill detection.

# 3 Oil spill detection method

## 3.1 Sea clutter statistical model

Sea clutter imaged by a low resolution radar system can be described by a complex Gaussian model [13]: when the radar illuminates a collection of independent scatterers, each of them contributes to the total field with single complex scattered fields. For a sufficiently large number of scatterers, the superposition principle applies and a Gaussian model can describe the sea clutter. The Gaussian model is no longer valid for high resolution SAR scenes, acquired by current and future SAR satellite systems. Indeed, in this case, larger fluctuations and sea spikes may be observed in a high resolution SAR image. The complex sea surface is characterized by many length scales, ranging from 1 centimeter or less to tens of meter. The shorter waves are independent within a high-resolution cell and give rise to speckle-like clutter. They are modulated by larger scale structures, which changes more slowly. Statistically this results in a locally Rayleigh process whose power is modulated by a random, independent, slowly varying process. This compound model for the sea clutter is then characterised by a non-Gaussian distribution. The probability density function (pdf) of the envelope $E$ of the Rayleigh process is:

$$P(E \setminus x) = \frac{2E}{x}\exp(-E^2/x); \qquad 0 \leq x \leq \infty \quad (2)$$

It is function of the local power $x$, which is itself a random variable with pdf $P_c(x)$. Thus the pdf of $E$ is obtained integrating (2) over $P_c(x)$, i.e.:

$$P(E) = 2E\int_0^\infty \frac{\exp(-E^2/x)}{x}P_c(x)dx \quad (3)$$

The equation (3) represents the compound form of the non-Gaussian clutter pdf. As stated in [13], a good model for $P_c(x)$ is the gamma distribution, which is function of the scale parameter, $b$ and shape parameter $\nu$:

$$P_c(x) = \frac{b^\nu}{\Gamma(\nu)}x^{\nu-1}\exp(-bx); \qquad 0 \leq x \leq \infty \quad (4)$$

Substituting the gamma distribution of local power (4) into the compound model expression, (3), the clutter envelope pdf can be determined, resulting in the K pdf [13].

## 3.2 Sea and oil simulation and detection

The proposed approach is based on the use of the sea and oil statistics. As introduced in the previous section, it is possible to simulate sea and oil statistical distribution by generating zero mean and unitary variance circular complex Gaussian samples $z$ as well as samples $a$ extracted from a gamma pdf, and after that, applying the compound model. The resulting samples, for both the co-polarimetric channels, are:

$$\begin{aligned}\sigma_{0_{VV}} &= a_{VV}\cdot z_{VV}\\ \sigma_{0_{HH}} &= a_{HH}\cdot z_{HH}\end{aligned} \quad (5)$$

In this analysis it is important to take into account the correlation between the two polarimetric channels. For the gaussian samples, which are related to the small scale sea structures, the correlation $\rho_z$ is expected to be higher for seawater than for oil covered areas [7]. They are parameter of the model that can be let varying accordingly to sea condition. Furthermore, for the larger scale phenomena, to a first approximation, no decorrelation has been assumed ($\rho_a = 1$). Consequently, the PR expected value is nothing else the ratio $a_{VV}/a_{HH}$. Sea and oil sampled distributions will also differ for the two parameter of the gamma pdf. The scale parameter is defined as the mean value divided by the shape parameter. Simulating data acquired by a C band system, the expected value of the distribution has been retrieved by the Radar Imaging Model, described in [9], that according to the weather condition (wind speed and direction), oil spill elasticity and for the two polarization channel provides the sea and oil $\sigma_0$ for a range of incidence angles (20-55 degrees). The free parameter for the gamma distribution is thus only the shape one: it affects the shape of the distribution and is expected to be higher for sea pdf than the oil one.

In **Figure 1** examples of two sample pdfs of the NRCS and PR for oil and sea are shown. They have been generated imposing the sea sample correlation $\rho_z = 0.9$, while that of oil samples has been fixed to $0.3$. Furthermore the shape parameter for the gamma pdf is equal to $7$ for sea and $2$ for oil. Moreover there have been assumed: incidence angle of $35$ degrees, wind speed of $8$ m/s and cross wind condition.

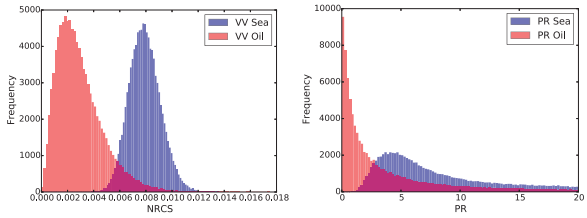


**Figure 1:** NRCS and PR sample pdfs for sea and oil computed with wind speed = $8$ m/s and cross wind, at incidence angle of $35$ degrees

Concerning the oil detection, the employed approach is based on the definition of a desired false alarm rate. Using a sample distribution both for the sea NRCS and PR, a proper threshold is estimated. Iterating with Monte Carlo simulations over many possible samples of sea and oil, the false alarm rate is evaluated as the number of sea samples below the threshold, over the total number of iterations. Similarly, the true positive rate is the number of oil samples below the threshold over the total number of iterations.

As shown in **Figure 2**, having fixed the incidence angle to $35$ degrees and with cross wind condition, varying the wind speed and for oil viscosity equal to $0.01$, the use of a CFAR detector only based on NRCS suffers from a higher probability of false alarm (even without generating samples of look-alikes). In the same conditions, the PR-based detector exhibits a lower value even though the probability of detection is higher for the RCS-based detector.

This motivates the use of a combined detector which exploits both the VV-NRCS and the PR in order to improve the performance, employing a double thresholding on the data.

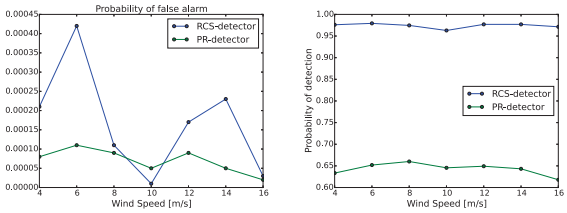


**Figure 2:** Probability of false alarm and detection for the CFAR detectors based on PR and NRCS, for different wind speeds and cross wind

First a threshold on the VV NRCS is employed and any cases for which $\sigma_0$ is lower than the threshold is classified as candidate oil spill; additionally, it must be lower than the PR-threshold. By doing so the probability of misclassification for a sea sample with a lower backscattering (as happen for the look-alikes) will be reduced. Similarly, the probability of detection of oil samples is increased: samples with RCS over the first threshold can still be recognized thanks to the PR information. **Figure 3** shows the improvements obtained by using the combined detector instead of one based on the RCS information alone.

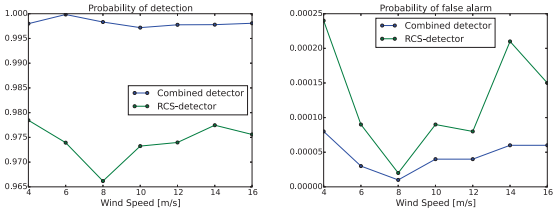


**Figure 3:** Probability of false alarm and detection for the NRCS-based CFAR detector and the combined one (PR and NRCS), for different wind speeds and cross wind

It is notable to observe that the performance is rather uniform for different wind speeds unlike what is usually expected, that as the wind speed exceed a medium value (around $10$ m/s) the detection capabilities are drastically reduced.

# 4 Real data results

Single Look Complex (SLC) images acquired over a selected test site in strip-map dual-pol (HH-VV) mode by the German satellite TerraSAR-X have been employed, aiming at proving the capability of the above described detectors. Given the image of interest and the required probability of false alarm, it is first of all, necessary to estimate a threshold: in this preliminary analysis a fixed threshold has been computed, basing on the sample distribution over a sufficiently large sea region included in the image. A threshold has been estimated according to the

ISBN 978-3-8007-4228-8 / ISSN 2197-4403

VV-NRCS distribution and another one on the PR, satisfying the required probability of false alarm. After that, a pixel wise comparison with respect to the threshold value is accomplished, labelling all the pixels in the image as sea / oil. The selected region includes an offshore platform 160 Km far away from Mumbai, India and has been already analyzed in the work [14]. **Figure 4** shows the VV-backscattering (left) and the corresponding PR (right) images, acquired in near range on 15th November 2014, and preprocessed with a $20 \times 20$ pixels multi-look window. The multi-look window size can affect the detector performance: a larger window reduces the speckle and consequently the probability of false alarm, but, at the same time this could imply the lost of very small oil spots that might be averaged out. In **Figure 5** the corresponding distributions for the entire scene are also displayed, both for the backscattering and the polarization ratio. It is notable that, as expected, the RCS histogram is bimodal exhibiting two different peaks related to the backscattering due to the sea and oil surfaces; similarly, the PR histogram has one lower peak around 1, identifying the oil pixels, and a higher one slightly displaced. The following images (see **Figure 6**) present the oil masks obtained by employing the oil detectors. Specifically, the masks on the top result respectively, from the use of a NRCS-based detector (figure on the left) and from the PR-based detector (on the right), having fixed for both the detectors a probability of false alarm equals to $0.001$. By comparing these last two images with the ones in **Figure 4** it is possible to notice that the RCS based detector allows the identification of the surfaces affected by oil. Nevertheless, a better detection capability thanks to the exploitation of the PR is remarkable: for example, an oil area on the left edge of the azimuth direction and between 4-6 km in range is recognizable only in the PR-based mask. In this last image, it is also possible to observe small spots in the left upper region, which might be ships, that are visible also in the PR image but not in the RCS one of **Figure 4**. The capability of some polarimetric features also for the identification of man-made objects in the sea has been addressed in the literature, but this lies outside the purpose of the current study. The possibility of using both the detector types to refine the detection capabilities is shown in **Figure 6** where the mask on the bottom, resulting by the combined use of the RCS and PR detector, shows an increased detection rate. Reducing the required probability of false alarm of one order of magnitude, the RCS-based detector is practically unable to recognize any oil slick, while the PR-based detector keep its detection capability; the combination of the two masks still allows the oil spills identification.

A different scenario is the one in **Figure 7** where the same region, but without oil slicks, acquired in far range on 17th July 2014, is presented. On the left the VV backscattering and on the right the Polarization Ration are shown. This is the case where look-alikes in the scene can be misclassified as oil. The use of the RCS based detector identifies some pixels in the scene as candidate oil spill; but they must be lower than the PR-threshold to be eventually classified as oil, according to the combined detector definition provided in the previous section. By using this double thresholding the probability of false alarm is strongly reduced. In this case rather than showing the sea / oil mask, which would not be very meaningful, the results are summarized in **Table 1**. The number of pixels that within the entire image are labelled as oil by the use of different detector kinds and for two different threshold values are reported. It can be noticed that in this scenario, the number the look-alikes is lower for the PR-based detector if compared to the RCS-based one. However, the combined detector is able to achieve the lowest number of pixel detected as oil. Furthermore, as it can be expected, the lower the probability of false alarm, the lower the number of pixel wrongly detected as oil.

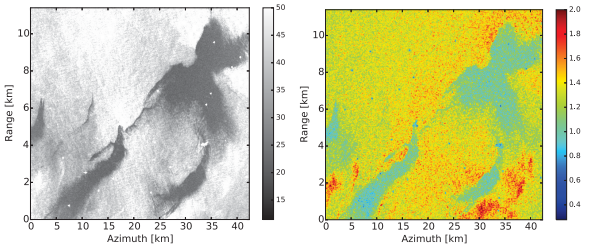


**Figure 4:** NRCS (VV Pol) TerraSAR-X image and corresponding PR

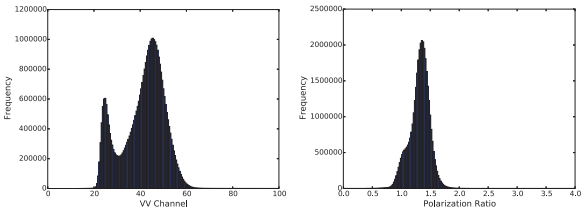


**Figure 5:** NRCS (VV Pol) and PR distribution

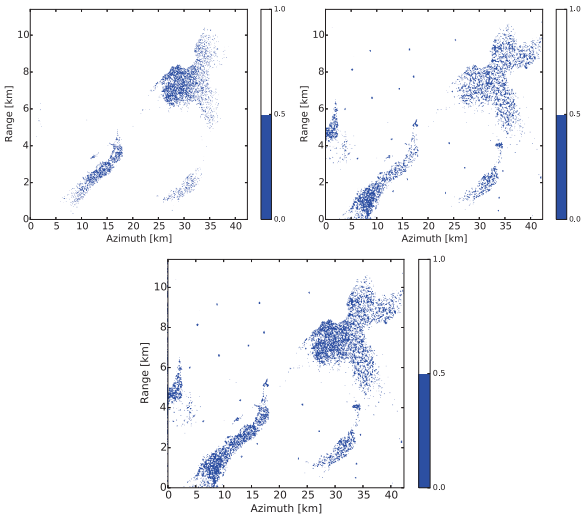


**Figure 6:** Oil slicks mask resulting from the application of the threshold based on the RCS (top left), PR (top right) and the combined use of the two (button)

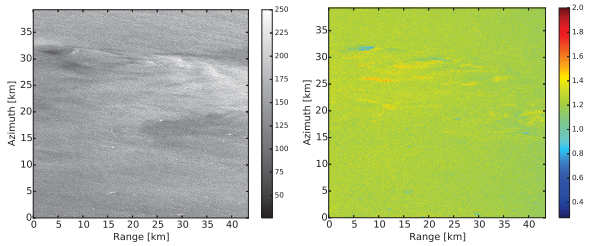


**Figure 7:** NRCS (VV Pol) TerraSAR-X image and corresponding PR

| $P_{fa}$ | RCS-Detector | PR-Detector | (RCS-PR)-Detector |
|---|---|---|---|
| $10^{-3}$ | 67932 | 42541 | 14924 |
| $10^{-4}$ | 2660 | 4760 | 266 |

**Table 1:** Number of pixel labelled as oil using the RCS or PR (only) detectors, and the combined one, for two different fixed probability of false alarm $P_{fa}$

# 5 Conclusions

This paper aims to compare a NRCS-based and a PR-based detectors with a combined one based on the information of both the NRCS and the PR. First of all, sea and oil high resolution SAR data have been simulated according to the compound model. The NRCS-based detector has shown higher probabilities of detection, but with lower probability of false alarm if compared to the PR-based detector. Our simulations have not yet explored the generation of look-alike conditions, which would be expected to increase the probability of false alarms.
Furthermore a simple combined CFAR detector, applying first a threshold on the NRCS and then on the PR, has demonstrate an improved capability to distinguish oil from seawater at different wind speeds. Anyway, the compound model on which the simulated data are based, does not take into account the breaking waves. They begin to be relevant above 10m/s, so that for higher wind speeds a falloff in the detection method can be expected.
The same method has been preliminarily tested on real TerraSAR-X data, acquired over areas affected by oil slicks. The use of the polarization ratio, jointly with the RCS, has revealed a strong potentiality, to be further analysed and exploited.
Furthermore, the exploitation simultaneous use of NRCS and PR information of SAR data by different kind of detectors, such as decision trees and clustering, to assess the best approach for spill detection, possibly for quasi real time applications, is still to be addressed.

# References

[1] M. F. Fingas and C. E. Brown: *Review of oil spill remote sensing*, Spill Science & Technology Bulletin, Vol. 4, No. 4, pp.199-208, 1997.

[2] C. Brekke, and A. H.S. Solberg: *Oil spill detection by satellite remote sensing*, Remote Sensing of Environment, Vol. 95, No. 1, pp.1-13, 2005.

[3] A. H. S. Solberg, G. Storvik, R. Solberg and E. Volden: *Automatic detection of oil spills in ERS SAR images*, IEEE Transactions on Geoscience and Remote Sensing, Vol. 37, No. 4, pp.1916-1924, 1999.

[4] T. F. N. Kanaa et al.: *Detection of oil slick signatures in SAR images by fusion of hysteresis thresholding responses*, Proceedings of IGARSS 2003, Vol. 4, pp.2750-2752, 2003.

[5] A. Gasull et al.: *Oil spills detection in SAR images using mathematical morphology*, Proceedings of EUSIPCO 2002, Vol. 1, pp.25-28 2002.

[6] V.N. Kudryavtsev, B. Chapron, A.G. Myasoedov, and F. Collard: *On dual co-polarized SAR measurements of the ocean surface*, IEEE Geoscience and Remote Sensing Letters, Vol. 10, No. 4, pp.761-765, 2013.

[7] M. Migliaccio, F. Nunziata and A. Gambardella: *On the co-polarized phase difference for oil spill detection*, International Journal of Remote Sensing, Vol. 30, No. 6, pp.1587-1602, 2009.

[8] S. Skrunes, C. Brekke, and T. Eltoft: *Characterization of marine surface slicks by Radarsat-2 multipolarization features*, IEEE Transactions on Geoscience and Remote Sensing, Vol. 52, No. 9, pp.5302-4762, 2014.

[9] V. Kudryavtsev, D. Hauser, G. Caudal, and B. Chapron: *A semi-empirical model of the normalized radar cross-section of the sea surface: 1. The background model*, Journal of Geophysical Research, Vol. 108, No. C3, 8054, 2003.

[10] F. G. Bass, I. M. Fuks, A. I. Kalmykov, I. E. Ostrovsky, and A. D. Rosenberg: *Very high frequency radiowave scattering by a disturbed sea surface, 2, Scattering from an actual sea surface*, IEEE Transaction on Antennas and Propagation, Vol. 16, pp.560-568, 1968.

[11] F. Girard-Ardhuin , G. Mercier, and R. Garello: *Oil slick detection by SAR imagery: potential and limitation*, Proceedings of OCEANS 2003, pp.164-169, 2003

[12] C. Brekke, B. Holt, C. Jones, and S. Skrunes: *Discrimination of oil spills from newly formed sea ice by synthetic aperture radar*, Remote Sensing of Environment, Vol. 145, pp.1-14, 2014.

[13] K. D. Ward, R. J. A. Tough and S. Watts: *Sea Clutter: Scattering, the K distribution and Radar Performance*, IET Radar, Sonar and Navigation Series 20, 2008.

[14] S. Singha, D. Velotto, S. Lehner: *Towards operational near real time oil spill detection service using polarimetrix TerreaSar-X Images*, Proceedings of POLINSAR 2015, pp. 1-6, 2015

ISBN 978-3-8007-4228-8 / ISSN 2197-4403  